ARTICLES
PUBLISHED ONLINE: 24 JULY 2011 | DOI: 10.1038/NGEO1212
nature geoscience

Non-mare silicic volcanism on the lunar farside at Compton–Belkovich

Bradley L. Jolliff[1]*, Sandra A. Wiseman[2], Samuel J. Lawrence[3], Thanh N. Tran[3], Mark S. Robinson[3], Hiroyuki Sato[3], B. Ray Hawke[4], Frank Scholten[5], Jürgen Oberst[5], Harald Hiesinger[6], Carolyn H. van der Bogert[6], Benjamin T. Greenhagen[7], Timothy D. Glotch[8] and David A. Paige[9]

Non-basaltic volcanism is rare on the Moon. The best known examples occur on the lunar nearside in the compositionally evolved Procellarum KREEP terrane. However, there is an isolated thorium-rich area—the Compton–Belkovich thorium anomaly—on the lunar farside for which the origin is enigmatic. Here we use images from the Lunar Reconnaissance Orbiter Cameras, digital terrain models and spectral data from the Diviner lunar radiometer to assess the morphology and composition of this region. We identify a central feature, 25 by 35 km across, that is characterized by elevated topography and relatively high reflectance. The topography includes a series of domes that range from less than 1 km to more than 6 km across, some with steeply sloping sides. We interpret these as volcanic domes formed from viscous lava. We also observe arcuate to irregular circular depressions, which we suggest result from collapse associated with volcanism. We find that the volcanic feature is also enriched in silica or alkali-feldspar, indicative of compositionally evolved, rhyolitic volcanic materials. We suggest that the Compton–Belkovich thorium anomaly represents a rare occurrence of non-basaltic volcanism on the lunar farside. We conclude that compositionally evolved volcanism did occur far removed from the Procellarum KREEP terrane.

The Compton–Belkovich thorium anomaly (CBTA), centred at 61.1° N, 99.5° E, was identified as an isolated thorium 'hotspot' in data obtained by the Lunar Prospector gamma-ray spectrometer (LP–GRS; Fig. 1; refs 1–3). The site has a high, focused concentration of thorium (Th) and is isolated in an area of Th-poor terrain on the lunar farside. It is nestled between two ancient impact craters, Compton (162 km diameter) and Belkovich (214 km diameter). Gillis and co-workers[4], using Clementine visible images, noted that the centre of the CBTA corresponds to an area of relatively high reflectance, about 30 km across. The elevated reflectance is readily apparent in Lunar Reconnaissance Orbiter Camera (LROC) Wide Angle Camera (WAC) images[5] (for example, Fig. 2a). The compositional anomaly in LP–GRS data is asymmetric and 'smeared' to the east, beyond the extent of the more highly reflective terrain (compare Figs 1 and 2). The Th anomaly covers a greater area than the high-reflectance terrain on which it is centred, but this results from the broad spatial response function of the LP–GRS (ref. 2) and is not a true representation of the areal extent of the Compton–Belkovich feature. Here, we investigate the high-reflectance feature (hereafter CBF) located at the centre of the CBTA—with images acquired by the WAC (100 m per pixel) and by the Narrow Angle Cameras (NACs) (0.5 to 1.5 m per pixel), with digital terrain data derived from NAC and WAC geometric stereo images, and with data acquired by the Diviner Lunar Radiometer Experiment on LRO.

LRO imaging and topography of the CBF

WAC images delineate the high-reflectance terrain covering an area of about 25 × 35 km from 98.5° to 101.0° E and 60.7° to 61.6° N (Fig. 2a). Within the high-reflectance terrain, reflectance is 20–40% higher on average than the surroundings in visible wavelengths (see Supplementary Information). The limited, contiguous extent of high-reflectance material indicates localization of the CBF; no large, contiguous patches of similarly reflective material occur beyond the main reflectance anomaly. A NAC-derived digital terrain model (DTM; ref. 6) shows locally elevated topography within the central region (Fig. 2c), including irregular depressions.

Topographic information derived from the WAC DTM (ref. 7; 100 m per pixel scale) and LOLA data[8] show that the CBF corresponds to an area of elevated topography (Fig. 3a,b). The central part of the topographic feature rises 400–600 m above the surrounding terrain, less on the west, where the CBF abuts mountains of the Belkovich crater rim, and greater to the east (Fig. 3a). The local elevation is approximately 2–3 km below the global mean surface elevation of 1,737.4 km. The site occurs in low terrain associated with the Humboldtianum basin, just inside its outer ring[4]. However, in this area the outer ring was obliterated by Compton, Belkovich, and other large, post-Humboldtianum impact events. The elevated topography (dashed outline in Fig. 2a) corresponds approximately, but not exactly, to the high-reflectance terrain. High-reflectance material extends ~5 km to the east-southeast of the boundary of the CBF elevated topography.

[1]Department of Earth and Planetary Sciences and the McDonnell Center for the Space Sciences, Washington University, One Brookings Drive, St Louis, Missouri 63130, USA, [2]Department of Geological Sciences, Brown University, Providence, Rhode Island 02912, USA, [3]School of Earth and Space Exploration, Box 871404, Arizona State University, Tempe, Arizona 85287, USA, [4]Hawaii Institute of Geophysics and Planetology, University of Hawaii, Honolulu, Hawaii 96822, USA, [5]German Aerospace Center (DLR), Institute of Planetary Research, Rutherfordstr. 2, D-12489 Berlin, Germany, [6]Institut für Planetologie, Westfälische Wilhelms-Universität Münster, Wilhelm-Klemm-Str. 10, 48149 Muenster, Germany, [7]Jet Propulsion Laboratory, 4800 Oak Grove Drive, M/S 183-301, Pasadena, California 91109, USA, [8]Department of Geosciences, Stony Brook University, Stony Brook, New York 11794, USA, [9]Department of Earth and Space Sciences, University of California, Los Angeles, California 90095, USA. *e-mail: blj@wustl.edu.

© 2011 Macmillan Publishers Limited. All rights reserved.

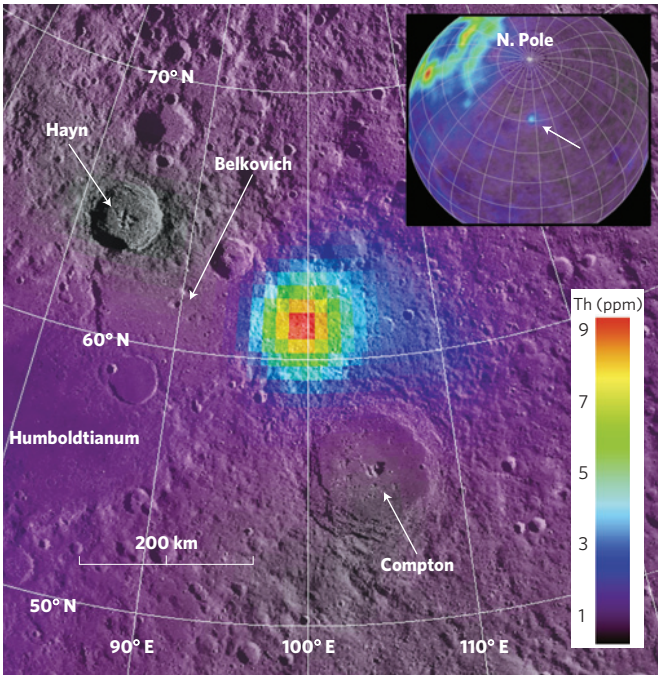

Figure 1 | Compton–Belkovich thorium anomaly. The location of the CBTA is northeast of Humboldtianum basin and just beyond the Moon's eastern limb (LP-GRS 0.5°, ~15 km resolution Th data[1,2] as deconvolved by Lawrence *et al.*[3], overlain on WAC 400 m per pixel base). The highest measured Th intensity corresponds to a concentration at this resolution of ~10 ppm at the centre of the Th hotspot.

Domes and irregular depressions

The elevated terrain is highest on the western and eastern flanks, reaching −1,800 m elevation, about 300–400 m above the central region (Fig. 3c, profile b–b′). In the north, at the edge of the high-reflectance terrain and CBF topographic feature, is an isolated massif over 6 km across at its base and nearly a kilometre high from base to summit. Its morphology suggests that it is volcanic in origin; its upper slopes range from 20 to 26° and it has a summit plateau with a broad, central depression (Fig. 4).

Just north-northeast of the CBF central depression, a north–south-oriented elongate rock body occurs with moderate relief (7°–22° slopes and 200 m above the base elevation, Fig. 2b). This feature, 2.5 km in length and ~2 km wide at its base, is probably also a volcanic construct (see also Fig. 4, 'middle dome'), but smaller than the massif ('big dome') to the north. Small channel-like features suggest flows and erosion occurred on its west side. Clusters of 1–5 m boulders are concentrated in several locations along its crest and flanks.

In and around the central area of the irregular depression marked '1' in Fig. 2b,c, small domes are also observed (for example, Fig. 2d). A half dozen small domes occur in the central area—all with similar size (~500 m across), but different morphologies, including some elongate forms and some that are subtle, low-relief bulges. Most have a prominent clustering of boulders at their summits and on their flanks (for example, Fig. 2e). The boulders are typically one to several metres in size, but some are as large as 10 m. Such clustering of boulders on domes has been noted in other locations, such as the Marius Hills[9]. The boulders suggest weathering of coherent rock as the domes degraded over time, with the largest boulders having been excavated by small impacts. In the example shown in Fig. 2d, the dome is ~500 m in diameter at the base and ~100 m high. The shape of the dome and its flank slopes, ~20°, indicate a more viscous lava composition (silicic) than expected for volcanic constructs associated with low-viscosity mare basalt lavas, which typically have slopes of <7° (ref. 10). Small domes such as these are found on Earth, associated with silicic (for example, rhyolitic) volcanism.

In addition to light-toned materials, numerous scarp-bounded irregular depressions occur in the CBF (Fig. 2b,d). Some of the irregular depressions form arcuate patterns (for example, Fig. 2c), although the central depression is not circular, and impact craters disrupt the boundary of the depression. In the irregular-shaped, central depressed area of the CBF, vertical relief on some of the scarps bounding collapse structures is ~50–100 m.

Bright material extends some 7 km to the E-SE beyond the region of elevated topography. Dispersal of bright material could be caused by impact cratering, and 7 km is a reasonable length scale for mixing from small impacts[11]. Another possibility is dispersal by pyroclastic eruption. The centre of a circle that fits the outline of this extension of bright material would be located in the depressed area labelled '3' in Fig. 2b, possibly a source vent. However, the high viscosity of this silicic magma may have favoured effusive eruption over pyroclastic eruption.

Possible rock types of the CBF

Using LP–GRS FeO and Th data, we investigate possible rock types that may be exposed in the CBF. Taking the low-altitude, two-degree binned data, a plot of FeO versus Th for the feature and surrounding regions shows the anomaly extending to about 3 ppm Th at about 5 wt.% FeO (refs 4,12; Fig. 5). The gamma-ray response function is broad (integrating the signal over a radius ~80 km, with a full-width half-maximum of 48 km for 30-km-altitude data[2]) such that the observed signal probably corresponds to a higher Th concentration and more focused areal extent than indicated by the first-reported data, as described by Lawrence and colleagues[2,3]. Lawrence *et al.*[2] modelled the CBTA as a highly localized source of high-Th material and concluded that the concentration of Th in the source materials at the centre of the CBTA could be as high as 40–55 ppm.

In Fig. 5, the LP–GRS data project toward high Th along vectors pointing to the compositions of two lunar rock types that are rare in the lunar sample collection: (1) granite or its fine-grained equivalent, felsite (rhyolite), and (2) the more mafic alkali norite or alkali gabbro (monzogabbro). These rock types are known only as small rocks and clasts in breccia, mainly in Apollo 12, 14, and 15 samples[13–18]. A pristine granitic rock fragment from Apollo 12 regolith[19,20] has the highest Th concentration measured so far in a lunar rock, 61 ppm, and an FeO concentration of 5 wt.%. Other lunar granites, however, have similarly enriched Th concentrations, typically in the 40–60 ppm range. The more mafic alkali-suite rocks also have elevated Th, but lower concentrations, for example, 10–40 ppm (refs 17,21). Alkali anorthosite could also be associated with these rocks, but typically has lower Th concentrations (Fig. 5). On the basis of compositions, silica- and feldspar-rich rocks would contribute to the high reflectance of the anomaly, especially granite or its extrusive equivalent, rhyolite.

Data from the LRO Diviner Lunar Radiometer[22] contribute another piece to the puzzle. The spectral signature measured by Diviner's three ~8-μm channels is consistent with highly polymerized mineralogy such as silica and/or alkali feldspar[23,24]. Quartz and K-feldspar are the two main mineralogical components of lunar granite, and no other common lunar minerals (olivine, pyroxene, anorthitic plagioclase, ilmenite, spinel) would create a similar signature in the Diviner data. An overlay of Diviner modelled Christiansen feature (CF) position in the 7.1–8.6 μm region (Fig. 6), which correlates inversely with silicate polymerization, shows a close correspondence between low CF modelled wavelength and the area of high reflectance. The CF modelled data demonstrate a better areal correspondence with the high-reflectance feature than with the topographic expression of the CBF. This observation supports

© 2011 Macmillan Publishers Limited. All rights reserved.

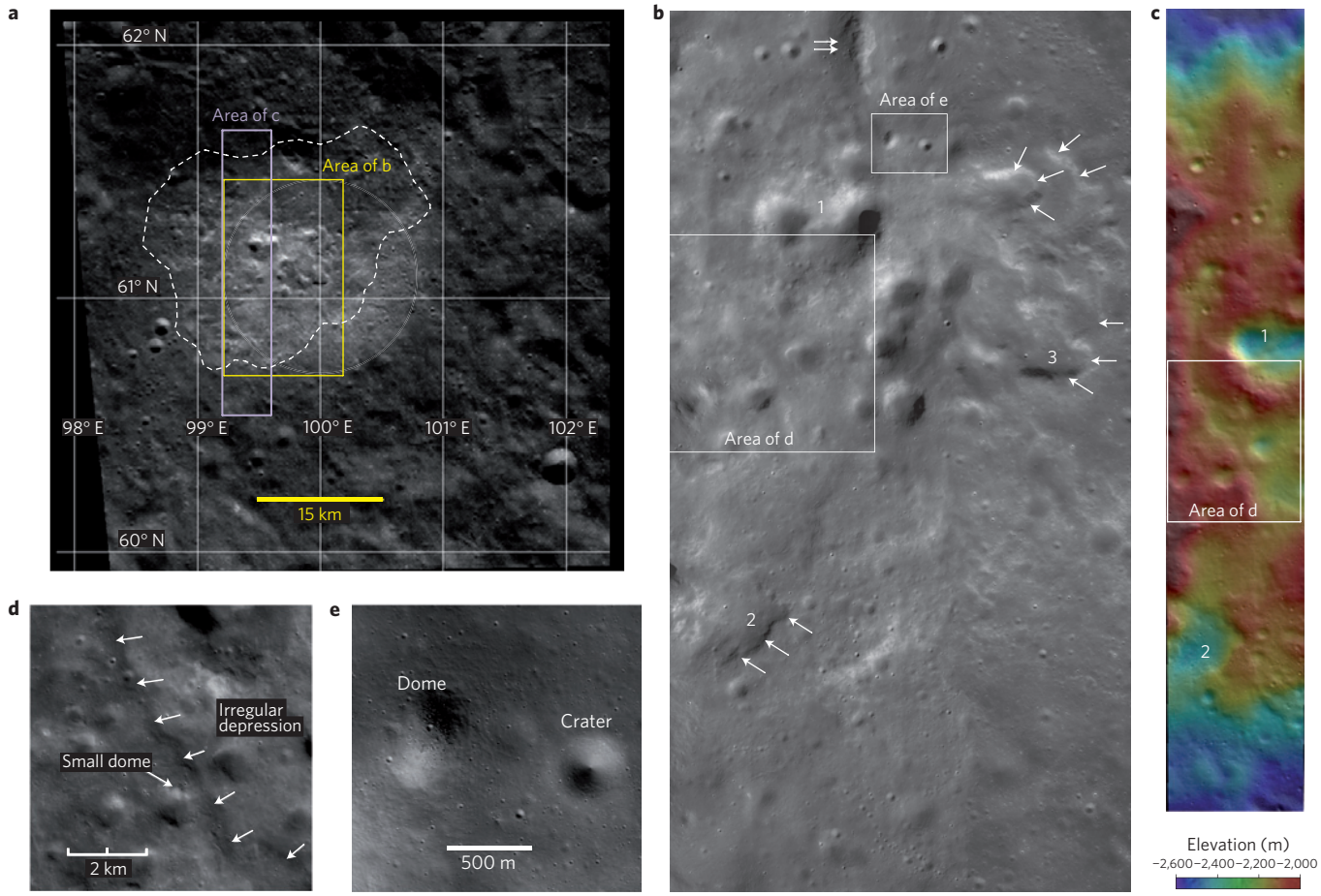

Figure 2 | Geomorphology of the CBF. a, Portion of WAC image showing high-reflectance terrain. Dashed outline denotes the topographically elevated area (Fig. 3). **b**, NAC mosaic showing the central region of the CBF and location of features discussed in text. Arrows indicate arcuate escarpments; double arrow locates the elongate rock body referred to in the text and Fig. 4 as 'middle dome.' Numbers 1 and 2 locate corresponding areas on parts **b** and **c**, 1, 2, and 3 correspond to irregular depressions (see text). **c**, Digital terrain model of the area noted in part **a**. **d**, Arcuate escarpment along the western side of the central depression. **e**, Small dome.

the possibility that silicic materials may have been distributed by pyroclastic eruption beyond the boundary of the topographic expression of the CBF, such as along its southeastern margin.

Origin of the CBF

Potential origins of the CBF include: (1) deposition as secondary ejecta, either from nearby (for example, Humboldtianum or Belkovich), or from far to the west (for example, as ejecta from the Imbrium impact event), or (2) exposure of a near-surface, isolated, alkali-intrusive/extrusive complex with high Th, but relatively low FeO, such as granite or alkali anorthosite[2,4]. The CBF bears no relationship to ejecta deposits and compositions of nearby large craters, nor is it co-located with obvious secondary craters, so a local impact-related origin is unlikely. Origin as an Imbrium ejecta deposit is unlikely because the inferred composition differs from other Imbrium ejecta, for example, Apollo 14 high-K KREEP rocks[21]. Moreover, the CBF and surrounding terrain lack elongation or 'sculpture' that would indicate an Imbrium source. Although located just east of the Belkovich crater rim, the CBF does not appear to be related to Belkovich rim deposits. The CBF is located along the extrapolated second ring of Humboldtianum basin; however, ring-related topography is absent in this region.

The data presented here are consistent with the CBF being an exposure of a near-surface, volcanic complex, including a central region that may be an irregularly shaped, collapsed caldera or set of vents. Accordingly, we infer that an initial hypabyssal (shallow) intrusion, possibly of KREEP-basalt or some similarly evolved composition, derived from melting deep in the crust, led to the local inflation or uplift of CBF topography, forming a low 'dome' some 30 km across and ~1 km high. As this lava solidified, it differentiated to produce more silicic residual melt and Th enrichment. Effusive eruptions produced elevated topography on the west and east sides of the CBF, and broad, low flow features. Late eruptives produced domes with slopes up to 26° and a range of sizes. As these positive relief volcanic features formed, other parts of the CBF collapsed, forming irregular-shaped calderas near the CBF centre. A small amount of late pyroclastic volcanism may have spread eruptive materials over a region extending to the southeast, some 7 km beyond the edge of the topographic feature.

The occurrence and preservation of small domes and other volcanic constructs suggest the CBF had not yet formed during the period of heavy impact bombardment. Ejecta deposits from Belkovich and Compton craters, which are Nectarian and Lower Imbrian, respectively[25], do not overprint the CBF, so the feature must postdate formation of these craters. Crater densities on several relatively flat areas within the CBF are conspicuously low, and preliminary crater counts suggest extraordinarily young ages, that is, Copernican; however, these apparently young surfaces need to be studied carefully to determine whether other characteristics, such as physical properties or specific surface characteristics, might affect small crater densities. Nonetheless, the good state of preservation of the CBF indicates that it has been little modified by impact processes.

© 2011 Macmillan Publishers Limited. All rights reserved.

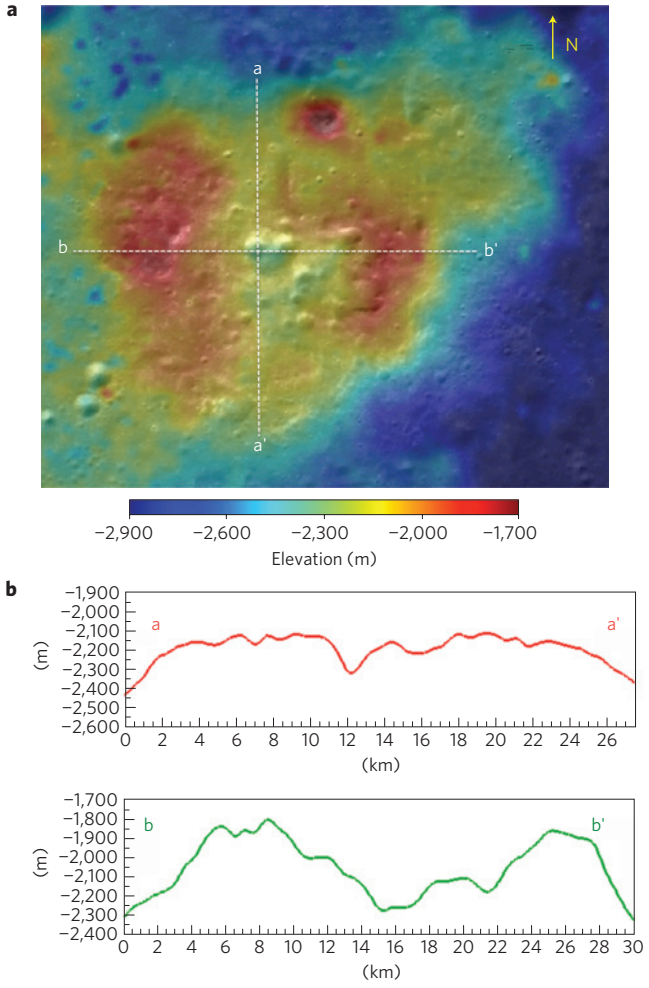

Figure 3 | Topography of the CBF. a, WAC DTM (200 m per pixel, draped over WAC orthophoto, 100 m per pixel). **b**, Elevation profiles for sections a–a′ and b–b′ generated from the WAC DTM.

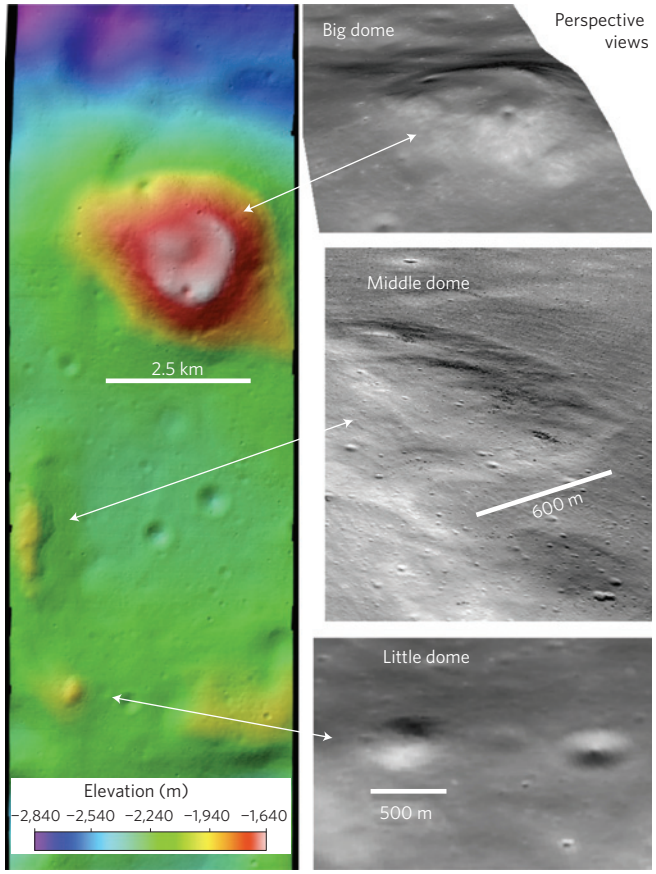

Figure 4 | Domes in the CBF. Positive relief features in the CBF inferred to be volcanic in origin.

On the basis of composition and morphologic features, we infer that the CBF represents a shallow, KREEP-rich (or similarly evolved) alkaline-silicic intrusive and volcanic complex. In the surrounding region, there is no evidence that any of the large impact craters excavated similar rock bodies, thus the magma source must have been deep in the crust, because there is no mechanism other than impact to heat shallow crustal rocks. It is unlikely, however, that a high-viscosity silicic magma would rise through a significant thickness of crust. A KREEP-basalt magma, derived from a more mafic intrusive or from a pocket of KREEP deep in the crust, however, could have intruded to shallow depth, perhaps ponding within the upper megaregolith layer, where extended differentiation produced late-stage, silicic residual melt that erupted to the surface. We postulate a relatively young intrusion (post Imbrium and perhaps much younger) and a deep source, because old, large impacts in the region, ranging from nearby 40 to 50 km diameter craters, to the large Compton and Belkovich craters, to Humboldtianum basin (650 km), do not appear to have tapped into or excavated enriched target rocks of KREEP-basalt or alkali-suite affinities.

The CBF lies distant, about 900 km to the east, from the Procellarum KREEP terrane[26], where compositionally evolved rocks are more common. This relative isolation indicates that within the lunar crust, and even well beyond the Procellarum KREEP terrane, mechanisms existed to produce compositionally and petrologically evolved lithologies late in crustal magmatic history, but that such occurrences are rare. Silicic magmas on the Moon require either extreme fractional crystallization of a KREEP-rich magma body with upward enrichment of silicic late-stage residual melt, or large-scale gravity separation of silicic melt from a magma that reached the field of silicate-liquid immiscibility during crystallization[21,27,28], producing conjugate mafic and felsic fractions, as occurs in some terrestrial mafic intrusives, such as the Skaergaard complex[29] in western Greenland.

Volcanism involving Th enrichment occurred in several locations on the lunar nearside within the Procellarum KREEP terrane, for example, Hansteen Alpha[30], the Gruithuisen domes[31,32], and the Lassell massif[24,33], and in several isolated locations on the lunar farside, for example, the Dewar region[2,34]. However, no other locations on the farside have such a prominent compositional signature, felsic mineralogy, and exposure as the CBF. The CBF is unusual because it is an example of non-mare volcanism, and it differs in its expression at the lunar surface, that is, a broad area of elevated topography with a range of volcanic features, including irregular depressions interpreted to be collapse features, small domes that can only be seen for the first time in the LROC NAC images, intermediate-sized domical volcanic features, and large volcanic constructs, the size of which approach the size of some of the Gruithuisen and Mairan domes[35].

Further questions are raised by the occurrence of the CBF. For example, how is this feature related to other nonmare volcanic features such as the Gruithuisen domes, and why does the CBF occur in such geographic isolation? Chevrel *et al.*[31] pointed out that because the Gruithuisen domes are embayed by mare basalt, the full expression of the volcanism that produced them could be more extensive. The CBF is not embayed by mare basalts, so the full extent of volcanism there is revealed. If the CBF formed relatively late in lunar magmatic evolution, what was the source

© 2011 Macmillan Publishers Limited. All rights reserved.

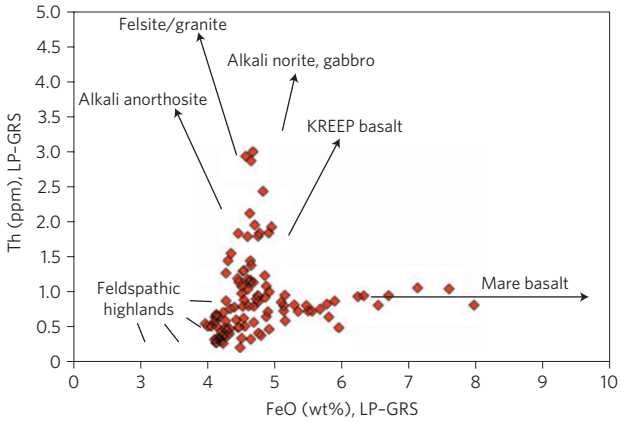

Figure 5 | Compositions of the CBTA and surrounding region. LP-GRS Th versus FeO for the region 80°–120° E and 50°–65° N. Low altitude, 2° binned data[1,2,8]. Vectors point to compositions of relevant lunar rock types[6,12–15,17]. The LP-GRS data in the Compton–Belkovich region are consistent with granite (rhyolite) or a mixture of granite and alkali anorthosite, norite and/or gabbro with well-mixed feldspathic highlands and basalt derived from nearby mare surfaces via impact processes.

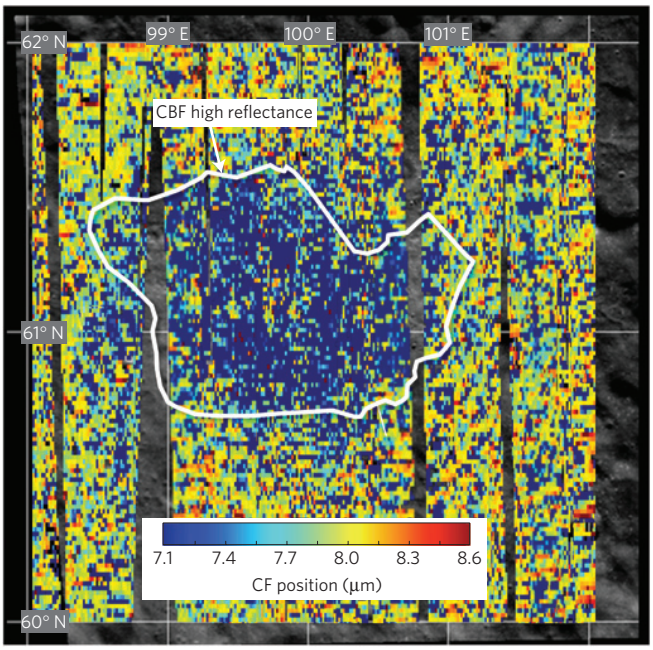

Figure 6 | Mineralogical information from LRO Diviner. Spectral data from Diviner showing the Christiansen feature position (7.1–8.6 μm; refs 22,23) overlain on an LRO WAC image. The red line represents the outline of the highly reflective area. The CF modelled data shown here as being more polymerized (blue) correspond more closely to the highly reflective terrain than to the topographically elevated area.

of heat that drove melting and how deep was it, was the parent melt similar to KREEP basalt, and how did the melt get to the surface? Crustal thickness models indicate that in the region of the CBF the crust is about 50 km thick[36]. Considering a two-layer model such as 'Model 3', shown by Wieczorek *et al.*[37], with a relatively thin (20 km) anorthositic upper crust and a similar or greater thickness of gabbroic lower crust, a melt of KREEP basalt composition and density could rise from the base of the crust to near the surface and pond at the base of, or within, a megaregolith several kilometres thick. Melt migration might have been aided by fracture or fault pathways associated with the second ring of Humboldtianum basin. In this regard, the CBF may be similar to the Gruithuisen volcanic complex, which is located along the second ring of Imbrium basin[31]. Chemical fractionation in the near-surface setting would then have permitted generation and further rise and extrusion of silicic magma, despite high viscosity, because it would have had only a short vertical distance to migrate.

Much remains to be learned about the Compton–Belkovich volcanic complex and how it relates to other occurrences of nonmare volcanism on the Moon. New, high-resolution imaging, determination of morphologies, and mineralogical remote sensing, which is possible with LRO and other recent mission results, reveal new insights to the Moon's past history and the extent of its geologic activity and variety, and pose new questions that could be addressed by renewed exploration of Earth's nearest and geologically complex neighbour.

Methods

LROC Images were processed using the Integrated Software for Imagers and Spectrometers (ISIS) produced by the US Geological Survey (http://isis.astrogeology.usgs.gov/TechnicalInfo/index.html) and Envi for post-processing display and processing of Digital Topographic Models (DTM). The LROC WAC image of Fig. 2 is M108555211CE, 566 nm, 66° incidence angle, and 69° phase angle. The DTM in Fig. 2, part c was derived from overlap of NAC pairs M108569083 and M108575940. The DTM used for Fig. 4 was derived from overlap of NAC pairs M139244929 and M139238146.

NAC DTMs. Procedures used to generate digital topographic models (DTMs) from NAC images are described by Tran and colleagues[38].

WAC DTM. Procedures used to generate the digital topographic model (DTM) from WAC images are described by Scholten and colleagues[39].

LRO Diviner Lunar Radiometer. Diviner-calibrated radiance data were binned at 64 pixels per degree and then converted to emissivity. The CF position was determined by fitting a parabola to the emissivity of the three 8-μm region channels. CF positions that occur shorter than Diviner's 8-μm region channels' range were assigned values of 7.0 μm. For additional details, the reader is referred to Greenhagen *et al.*[23] and Glotch and colleagues[24].

Received 24 March 2011; accepted 22 June 2011; published online 24 July 2011

References

1. Lawrence, D. J. *et al.* High resolution measurements of absolute thorium abundance on the lunar surface. *Geophys. Res. Lett.* **26,** 2681–2683 (1999).
2. Lawrence, D. J. *et al.* Small-area thorium features on the lunar surface. *J. Geophys. Res.* **108,** JE002050 (2003).
3. Lawrence, D. J. *et al.* Global spatial deconvolution of Lunar Prospector Th abundances. *Geophys. Res. Lett.* **34,** L03201 (2007).
4. Gillis, J. J., Jolliff, B. L., Lawrence, D. J., Lawson, S. L. & Prettyman, T. H. The Compton–Belkovich region of the Moon: Remotely sensed observations and lunar sample association. *Lunar Planet. Sci.* **33,** abstr. no. 1967 (2002).
5. Robinson, M. S. *et al.* Lunar Reconnaissance Orbiter Camera (LROC) instrument overview. *Space Sci. Rev.* **150,** 81–124 (2010).
6. Tran, T. *et al.* Generating digital terrain models from LROC stereo images with SOCET SET. *Lunar Planet. Sci.* **41,** abstr. no. 2515 (2010).
7. Scholten, F. *et al.* Towards global lunar topography using LROC WAC stereo data. *Lunar Planet. Sci.* **41,** abstr. no. 2111 (2010).
8. Zuber, M. T. *et al.* The Lunar Orbiter Laser Altimeter investigation on the Lunar Reconnaissance Orbiter mission. *Space Sci. Rev.* **150,** 63–80 (2010).
9. Lawrence, S. J. *et al.* LROC observations of the Marius Hills. *Lunar Planet. Sci.* **41,** abstr. no. 1906 (2010).
10. Murase, T. & McBirney, A. R. Viscosity of lunar lavas. *Science* **167,** 1491–1493 (1970).
11. Li, L. & Mustard, J. F. Compositional gradients across mare-highland contacts: Importance and geological implication of lateral transport. *J. Geophys. Res.* **105,** 20431–20450 (2000).
12. Lawrence, D. J. *et al.* Iron abundances on the lunar surface as measured by the Lunar Prospector gamma-ray and neutron spectrometers. *J. Geophys. Res.* **107,** JE001530 (2002).
13. Ryder, G. Lunar sample 15405: Remnant of a KREEP basalt-granite differentiated pluton. *Earth Planet. Sci. Lett.* **29,** 255–268 (1976).
14. Warren, P. H. *et al.* Seventh foray: Whitlockite-rich lithologies, a diopside-bearing troctolitic anorthosite, ferroan anorthosites, and KREEP. *Proc. Lunar Planet. Sci. Conf. 14th in J. Geophys. Res.* **88,** B151–B164 (1983).

© 2011 Macmillan Publishers Limited. All rights reserved.

15. Warren, P. H., Jerde, E. A. & Kallemeyn, G. W. Pristine Moon rocks: A 'large' felsite and a metal-rich ferroan anorthosite. *Proc. Lunar. Planet. Sci. Conf. 17th in J. Geophys. Res.* **92,** E303–E313 (1987).
16. Marvin, U. B., Lindstrom, M. M., Holmberg, B. B. & Martinez, R. R. New observations on the quartz monzodiorite-granite suite. *Proc. Lunar Planet. Sci.* **21,** 119–135 (1991).
17. Jolliff, B. L. Fragments of quartz monzodiorite and felsite in Apollo 14 soil particles. *Proc. Lunar Planet. Sci.* **21,** 101–118 (1991).
18. Snyder, G. A., Taylor, L. A. & Halliday, A. Chronology and petrogenesis of the lunar highlands alkali suite: Cumulates from KREEP basalt crystallization. *Geochim. Cosmochim. Acta* **59,** 1185–1203 (1995).
19. Seddio, S. M., Jolliff, B. L., Korotev, R. L. & Zeigler, R. A. A newly characterized granite from the Apollo 12 regolith. *Lunar Planet. Sci.* **40,** abstr. no. 2285 (2009).
20. Seddio, S. M., Korotev, R. L., Jolliff, B. L. & Zeigler, R. A. Comparing the bulk compositions of lunar granites, with petrologic implications. *Lunar Planet. Sci.* **41,** abstr. no. 2688 (2010).
21. Jolliff, B. L. Large-scale separation of K-frac and REEP-frac in the source regions of Apollo impact-melt breccias, and a revised estimate of the KREEP composition. *Int. Geology Rev.* **40,** 916–935 (1998).
22. Paige, D. A. *et al.* The Lunar Reconnaissance Orbiter Diviner Lunar Radiometer Experiment. *Space Sci. Rev.* **150,** 125–160 (2010).
23. Greenhagen, B. T. *et al.* Global silicate mineralogy of the Moon from the Diviner lunar radiometer. *Science* **329,** 1507–1509 (2010).
24. Glotch, T. D. *et al.* Identification of highly silicic features on the Moon. *Science* **329,** 1510–1513 (2010).
25. Wilhelms, D. E. in *The geologic history of the Moon* Vol. 1348 (US Geol. Surv. Prof. Paper, United States Government Printing Office, 1987).
26. Jolliff, B. L., Gillis, J. J., Haskin, L., Korotev, R. L. & Wieczorek, M. A. Major lunar crustal terranes: Surface expressions and crust-mantle origins. *J. Geophys. Res.* **105,** 4197–4216 (2000).
27. Taylor, G. J., Warner, R. D., Keil, K., Ma, M-S. & Schmitt, R. A. in *Proceedings of the Conference on the Lunar Highlands Crust* (eds Papike, J. J. & Merrill, R. B.) 339–352 (*Geochim. Cosmochim. Acta*: Supplement, 12, Pergamon, 1980).
28. Longhi, J. Silicate liquid immiscibility in isothermal crystallization experiments. *Proc. Lunar Planet. Sci. Conf.* **20,** 13–24 (1990).
29. McBirney, A. R. & Nakamura, Y. Immiscibility in late-stage magmas of the Skaergaard intrusion. *Carnegie Inst. Wash. Yearb.* **73,** 348–352 (1974).
30. Hawke, B. R. *et al.* Hansteen Alpha: A volcanic construct in the lunar highlands. *J. Geophys. Res.* **108,** E002013 (2003).
31. Chevrel, S. D., Pinet, P. C. & Head, J. W. III Gruithuisen domes region: A candidate for an extended nonmare volcanism unit on the Moon. *J. Geophys. Res.* **104,** 16515–16529 (1999).
32. Wilson, L. & Head, J. W. Lunar Gruithuisen and Mairan domes: Rheology and mode of emplacement. *J. Geophys. Res.* **108,** 5012 (2003).
33. Hagerty, J. J. *et al.* Refined thorium abundances for lunar red spots: Implications for evolved, nonmare volcanism on the Moon. *J. Geophys. Res.* **111,** E06002 (2006).
34. Lawrence, S. J. *et al.* Composition and origin of the Dewar geochemical anomaly. *J. Geophys. Res.* **113,** E02001 (2008).
35. Tran, T. *et al.* Morphometry of lunar volcanic domes from LROC. *Lunar Planet. Sci.* **42,** abstr. no. 2228 (2011).
36. Wieczorek, M. A. & Phillips, R. J. Potential anomalies on a sphere: Application to the thickness of the lunar crust. *J. Geophys. Res.* **103,** 1715–1724 (1998).
37. Wieczorek, M. A. *et al.* in *New Views of the Moon* Vol. 60 (eds Jolliff, B. L., Wieczorek, M. A., Shearer, C. K. & Neal, C. R.) 221–364 (Mineralogical Society of America, 2006).
38. Tran, T. *et al. Generating digital terrain models using LROC NAC images. Joint Symposium of ISPRS Technical Commission IV & AutoCarto in conjunction with ASPRS/CaGIS 2010 Fall Specialty Conference*, Nov. 15–19, Orlando, Florida.
39. Scholten, F. *et al.* Towards global lunar topography using LROC WAC stereo data. *Lunar Planet. Sci.* **41,** abstr. no. 2111 (2010).

Acknowledgements

The authors thank the LRO, LROC, and Diviner operations teams for their work and NASA ESMD and SMD for support of the LRO mission. The authors thank N. Petro for comments, which led to significant improvements in the manuscript.

Author contributions

B.L.J. drafted the initial manuscript. S.A.W. processed WAC images and DTMs, and assisted with NAC image processing. S.J.L. worked with B.L.J. on the topic of lunar red spots and volcanic domes. M.S.R is the principal investigator of the LRO Cameras, was responsible for development and operation of the camera system, and contributed to scientific interpretations. F.S. and J.O. of DLR derived and provided the WAC DTM. T.N.T. processed and provided the NAC DTMs and first characterized the 'big dome.' S.J.L., M.S.R., B.R.H., H.H., and C.H.v.d.B. provided input on geological relationships and contributed to writing the paper. H.S. provided data for reflectance analysis. B.T.G. and D.A.P. provided the Diviner data, T.D.G. contributed to interpretation of the CF, and D.A.P. is the principal investigator of the Diviner lunar radiometer. All of the authors contributed to assessment and discussion of the results.

Additional information

The authors declare no competing financial interests. Supplementary information accompanies this paper on www.nature.com/naturegeoscience. Reprints and permissions information is available online at http://www.nature.com/reprints. Correspondence and requests for materials should be addressed to B.L.J

© 2011 Macmillan Publishers Limited. All rights reserved.